JOURNAL OF APPLIED POLYMER SCIENCE VOL. 20, 1823–1847 (1976)

The Influence of Drawing, Twisting, Heat Setting, and Untwisting on the Structure and Mechanical Properties of Melt-Spun High-Density Polyethylene Fiber

GORDON M. SZE, JOSEPH E. SPRUIELL, and JAMES L. WHITE,
Department of Chemical and Metallurgical Engineering, The University of Tennessee, Knoxville, Tennessee 37916

Synopsis

The variation of crystalline morphology and mechanical properties of polyethylene fibers was studied as they were sequentially melt spun, drawn, twisted, heat set, and untwisted. Twisting of as-melt spun fibers was also investigated. The morphology was characterized using wide-angle x-ray diffraction, small-angle x-ray diffraction, and scanning electron microscopy techniques. Drawing results in high crystalline orientation, fibrillation, and large increases in modulus and tensile strength. Effects due to variation of spinning conditions were noted. Twisting either as-spun or drawn fibers decreased the axial orientation, modulus, tensile strength, and usually also the elongation to break. The changes in these properties increased with twist angle. Twisting also caused transformation of a small fraction of the sample to the monoclinic form of polyethylene. Heat setting caused healing of voids generated during drawing and increased the perfection and periodicity of the stacking of lamellar crystals along the fiber axis. Heat setting also caused the monoclinic polyethylene to transform back to the orthorhombic form, and it increased the modulus and tensile strength. Untwisting returned the orientation in the fiber to essentially that which it would have if it had not been twisted, but untwisting also resulted in the formation of kink bands.

INTRODUCTION

It is well known that the structure and mechanical properties of melt-spun fibers vary considerably as they are drawn, twisted, and heat set in successive processing stages. Twisting of fibers occurs in the preparation and handling of yarns[1,2] and in false twist texturing.[3–5] The development of orientation and tensile strength of fibers on drawing was first shown by Carothers and Hill.[6] More recently, it has been realized that drawing processes are also accompanied by fibrillation.[7–10] Deformations of oriented crystalline polymers such as drawn fibers are known to lead to phenomena such as the formation of kink bands[11–15] and polymorphic phase transformations.[16–18]

Experimental studies of the stretching of fibers and films usually begin with carefully prepared isotropic samples. The few investigations of structural changes in twisting by Cooper and his colleagues[18–20] though of high quality begin with commercial fibers melt spun and drawn under unknown

conditions. There seems to be no study in the literature where the variation in structure and mechanical properties are followed through:

melt spinning → drawing → twisting → heat setting → untwisting

or

melt spinning → twisting → drawing.

We shall describe such a research study in this paper for high-density polyethylene fibers. The reasons for studying polyethylene are its well-known and well-formed crystalline character, including a relatively simple orthorhombic unit cell[21] and a high level of crystallinity. In addition, polyethylene is chemically stable and not influenced by moisture. This paper continues earlier studies from the University of Tennessee on melt spinning and drawing of fibers.[22–28] In part of this work,[25–27] we have looked in some detail at the development of structure and mechanical properties in melt-spun polyethylene fibers. The paper of White, Dharod, and Clark[27] contains initial studies of the drawing of polyethylene fibers and the interaction between melt spinning and drawing.

EXPERIMENTAL

Materials

A series of melt-spun high-density polyethylene (HDPE) filaments previously prepared by Dees and Spruiell[26] were used for these studies. The polymer was a Phillips Marlex EMB 6050 with nominal melt index 5.0. Two samples, labeled PE01 and PE07, differing greatly in take-up velocity and stress developed in the spinline, were chosen for the majority of the research. Some studies also included a very low take-up velocity sample PE03. Only cursory examination was given to other spinning conditions. The detailed spinning conditions for the three fibers are summarized in Table I.

Deformation and Heat Setting of Fibers

Drawing was carried out at 24°C using an Instron Universal Testing Machine. A predetermined length of fiber was clamped between the Instron

TABLE I
Spinning Conditions of High-Density Polyethylene Fibers

Name	PE03	PE01	PE07
Extrusion rate, g/min	1.93 ± 0.03	1.93 ± 0.03	1.93 ± 0.03
Melt temperature, °C	205	205	210
Take-up velocity, m/min	50	100	556
Spinning stress, (dynes/cm^2) × 10^{-6}	1.0	2.8	17.1
Ambient temperature, °C	28.0	28.0	28.5
Diameter, cm	0.0220	0.0179	0.0063

grips; the cross head was then set in motion at a speed calculated to produce a drawing rate of 50% per minute.

Twisting of either as-spun or drawn fibers was carried out in a Twist Tester (Alfred Suter Company, New York) under constant load. One of the two grips was hooked to a 10-g load through the use of a pulley. This allowed the grip to move to provide for reduction in fiber length as twisting proceeded. The other grip was fixed and connected to a twisting handle through a set of gears such that each full turn of the handle caused the grip to make 10 full revolutions. A meter connected to the twisting handle provided a means for counting the total number of turns introduced into the length of fiber between the two grips.

Fibers were annealed in a temperature-controlled oven. All annealing treatments were for 30 min at 120°C.

Characterization of Fiber Structure

Three major tools were used to investigate the structure of the polyethylene fiber processed in this study. These are scanning electron microscopy (SEM), small-angle x-ray diffraction (SAXS), and wide-angle x-ray diffraction (WAXS). The three instruments provide information on different structural levels. The SEM allows examination of fiber surface features in the micron (10^4 angstroms) size range with high contrast and great depth of focus. By use of a peeling technique,[10,29,30] the internal structure of the fibers may also be viewed. SAXS patterns relate to structural characteristics in the size range of tens to hundreds of angstroms.[31] WAXS patterns are determined by structural features at the level of a few angstrom units and provide information on the extent of crystallinity and of the character of the orientation of the crystalline regions.[31]

The SEM studies were carried out using an AMR Model 900 high-resolution scanning electron microscope (Advanced Metals Research Corporation, Burlington, Massachusetts). A gold–palladium alloy coating was used on the fibers to eliminate charging in the electron beam.

Wide-angle x-ray diffraction patterns were recorded on flat film using a Rigaku-General Electric rotating anode x-ray generator. The sample-to-film distance was 1.85 cm. The radiation used was nickel-filtered copper K_α of wavelength 1.542 angstrom units. The x-ray unit was operated at 50 kV and 80 ma.

Small-angle x-ray patterns were obtained using a custom-made collimator mounted in a Kiessig camera. With the pinholes used in the present work, this custom-made collimator provided a resolution of about 400 angstroms. The camera was evacuated by a mechanical vacuum pump to reduce air scattering. The sample-to-film distance was 400 mm.

Mechanical Property Measurements

The mechanical properties of the fibers studied were determined using an Instron Universal Testing Machine. The initial gauge length of the fiber was maintained at 1 in., and the tests were all run at room temperature (24°C) at a cross-head speed of 1 in./min. Extreme care was taken in mounting the fi-

bers in the grips. A special fixture was developed for transferring twisted fibers from the twist tester so that the twist level could be maintained.

The tensile strength quoted in this paper is defined as the force at fracture divided by the original cross-sectional area of the fiber. The elastic modulus is Young's tangent modulus defined by

$$E = \lim_{\epsilon \to 0} \frac{\Delta \sigma}{\Delta \epsilon} \tag{1}$$

where σ is the engineering stress and ϵ is the engineering strain.

RESULTS AND DISCUSSION

As-Spun Filaments

In Figure 1, we show scanning electron micrographs of filaments spun at three different take-up velocities, 50 m/min (PE03), 100 m/min (PE01), and 556 m/min (PE07). Figure 2 shows WAXS and SAXS patterns for PE01 and PE07. The SEM photomicrographs show no remarkable features, beyond some minor surface roughness which seems to decrease in prevalence as the take-up velocity increases. The SAXS patterns show two-point meridional discrete scattering indicative of periodic variations of electron density along the fiber axis. The WAXS patterns indicate high levels of crystallinity and orientation in both filaments. The 020 reflections for both cases are concentrated near the equator, indicating that the b-axes of the polyethylene crystals are essentially perpendicular to the fiber axis. Dees and Spruiell[26] quantitatively analyzed similar diffraction patterns from the same samples used in this study. Computed SAXS long periods, crystallinities, and the Hermans-Stein crystalline factors[25–27,32–34] are summarized in Table II. The orientation factors are a measure of the average position of the crystallographic axes of the polyethylene crystals relative to the fiber axis. They are defined in such a way that f_x will be unity if the x-crystallographic axes are all parallel to the fiber axis, $f_x = -0.5$ if the x-crystallographic axes are perpendicular to the fiber axis and $f_x = 0$ for a random orientation.

Figure 3 shows typical engineering stress versus strain curves for the PE01 and PE07 as-spun fibers. The PE07 fiber exhibits a higher modulus and tensile strength than PE01, but a smaller elongation to break. The results are also summarized in Table II.

Previous studies of polyethylene using these and similar tools have given rise to some understanding of the structure of this material on various levels and this will be of considerable utility in interpretation of our experiments. Keller,[35] on the basis of electron-microscopic studies of polymer single crystals[35,36] and SAXS repeat distances, suggested that crystalline polyethylene in the bulk state consists of folded-chain lamellae. Such an explanation is able to explain the birefringent character of spherulites[37–39] through the idea of twisting folded-chain lamellae growing from a nucleus. On the basis of electron microscope studies of structure formed from stirred dilute solutions,[40] SAXS patterns, and azimuthal variations in intensity of WAXS patterns, Keller and Machin[41] proposed that stressed melts of polyethylene and other polymers crystallize in the form of *row structures* which consist of par-

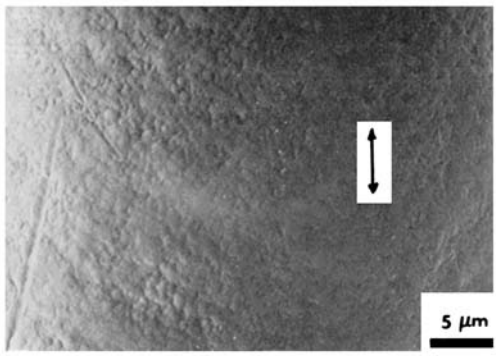

(a)

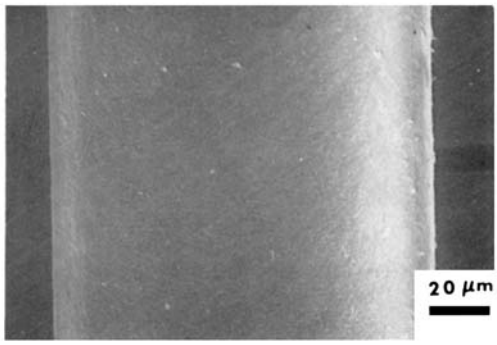

(b)

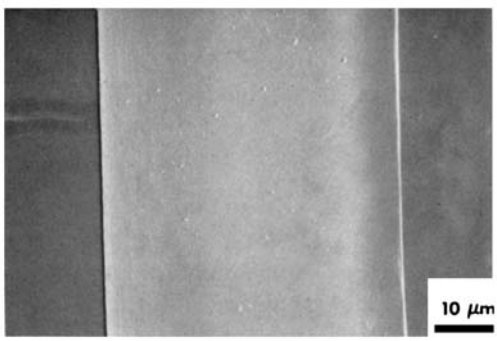

(c)

Fig. 1. Scanning electron micrographs of as-spun HDPE filaments: (a) PE03, take-up velocity of 50 m/min; (b) PE01, take-up velocity of 100 m/min; (c) PE07, take-up velocity of 556 m/min.

allel rows of folded-chain lamellae. Dees and Spruiell[26] used this model to interpret the morphology of these as-spun polyethylene filaments. Their model is shown in Figure 4. The lamellae are presumed to nucleate on fibril nuclei and grow radially outward, the growth direction being the b-axis direction in polyethylene. At low stresses, the lamellae twist about this axis as they grow outward; a feature which accounts for the nearly equal orientation factors for a- and c-axes in the PE01 sample, Table II. In the PE07 sample spun under much higher spinline stress, f_a decreases as f_c increases. This behavior is consistent with less twisting of the folded-chain lamellae.

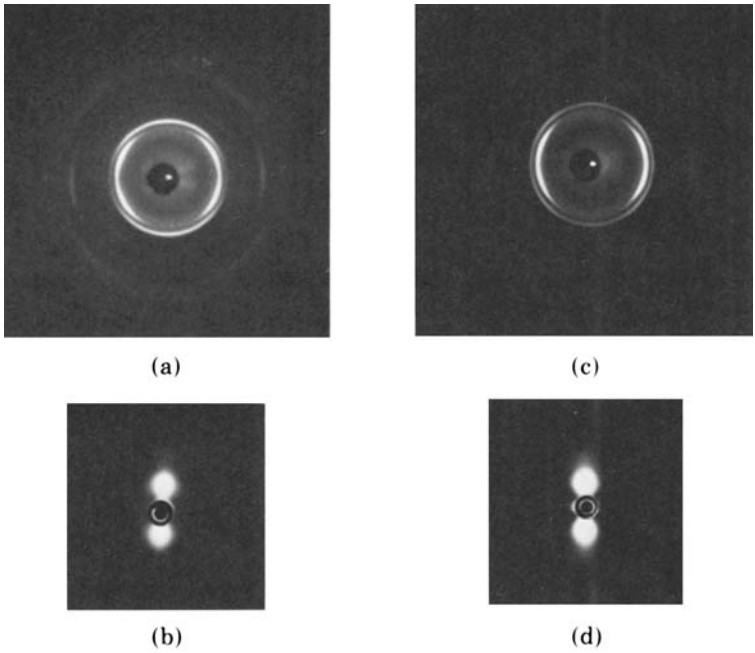

Fig. 2. X-ray diffraction patterns of as-spun HDPE filaments: (a) WAXS, PE01; (b) SAXS, PE01; (c) WAXS, PE07; (d) SAXS, PE07.

There are probably other more subtle changes in morphology with change of take-up velocity and spinning stress such as changes in the perfection of the lamellar crystals, the number and type of tie molecules, etc. All of these changes taken together cause the very significant difference in mechanical properties observed in Figure 3 and Table II.

Drawn Fibers

The drawing characteristics of the melt-spun fibers varied considerably. As already noted in the mechanical property data given in Table II, the maximum draw ratio (DR at break) varied from about 19 for the PE03 fiber spun at 50 m/min to 15 for PE01 spun at 100 m/min to 7 for PE07 spun at 556 m/min.

Necks and shoulders were found to develop in the fibers during the cold-drawing operation. We define the natural draw ratio, NDR, as the draw ratio required for all necks and shoulders to disappear. The PE03 fiber had an

TABLE II
Structure and Mechanical Properties of Melt-Spun Fibers

Sample	SAXS long period Å	Crystallinity, %	f_a	f_b	f_c	Young's tangent modulus, dynes/cm²	Tensile strength, dynes/cm²	Elongation to break, %
PE03	247	63.4	0.26	−0.39	0.13	9.2×10^9	3.6×10^8	1800
PE01	239	62.3	0.22	−0.42	0.20	9.4×10^9	4.0×10^8	1400
PE07	229	57.7	−0.28	−0.40	0.68	18.8×10^9	11.0×10^8	600

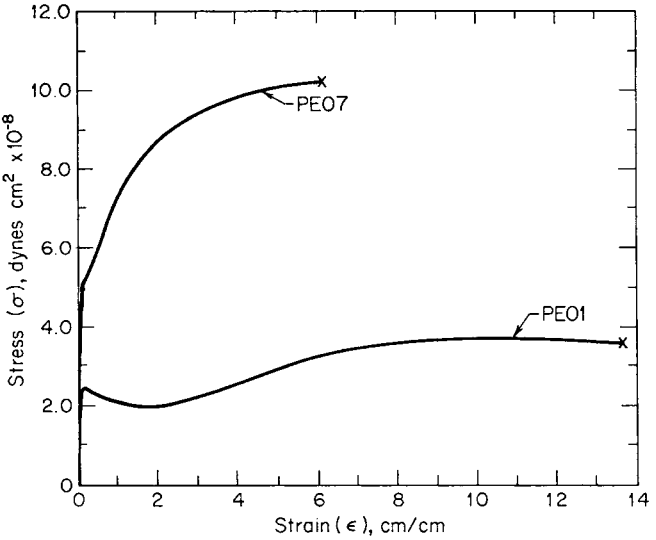

Fig. 3. Typical stress–strain (σ–ϵ) curves for the melt-spun filaments.

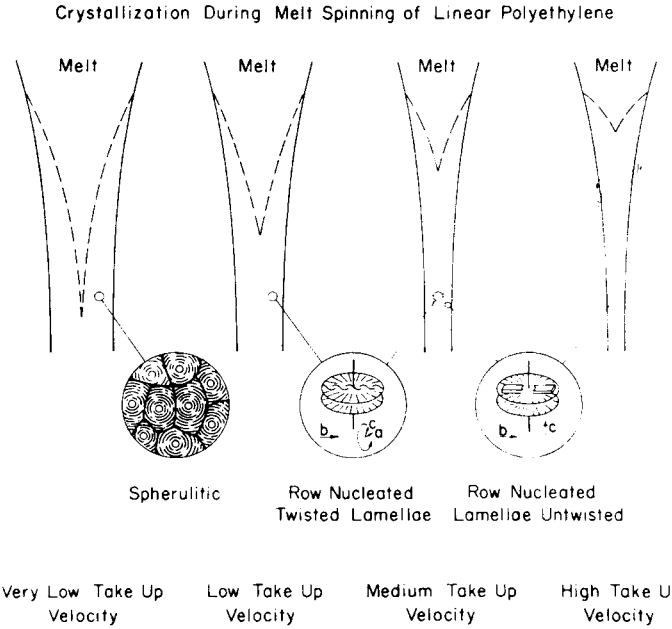

Fig. 4. Structure model proposed by Dees and Spruiell[26] for melt-spun HDPE filaments. The model is based on the row structure models of Keller and Machin.[41]

NDR of 5.2, the PE01 an NDR of 3.0, and the PE07 a very low NDR (less than 2). Thus, the NDR, like maximum draw ratio, decreases with increasing spinline take-up velocity and/or stress.

In Figures 5 and 6, we show SEM photomicrographs and SAXS and WAXS patterns for the PE01 fiber at draw ratio 10 and the PE07 fiber at draw ratio 4. It is clear from the SEM photomicrographs that the drawn fibers have a fibrillar superstructure.

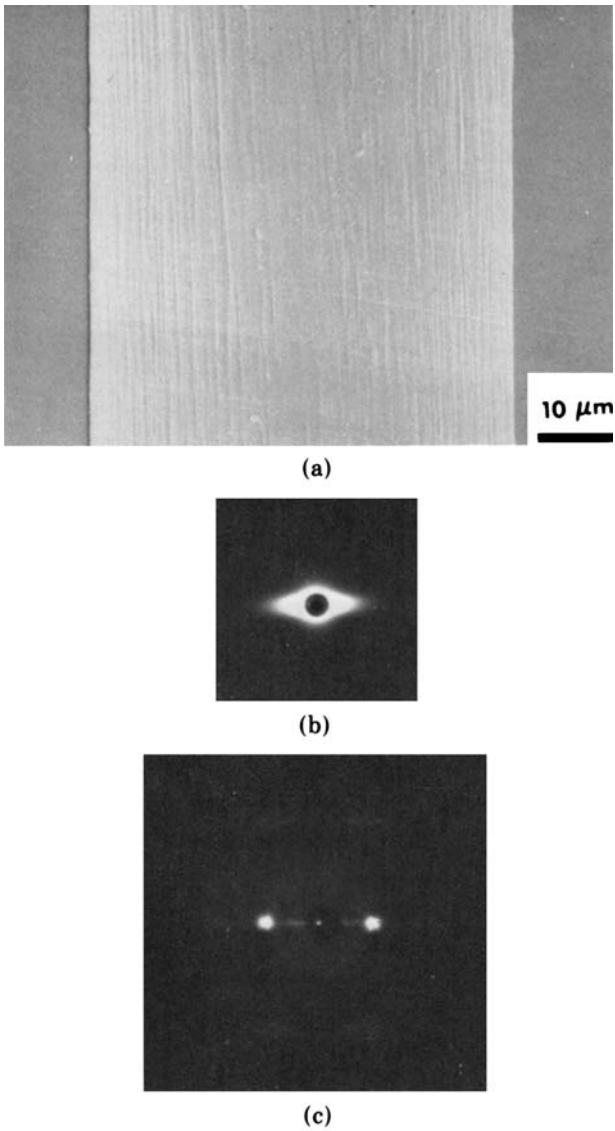

Fig. 5. Characterization of drawn (10×) PE01 fibers: (a) SEM photomicrograph; (b) SAXS pattern; (c) WAXS pattern.

The SAXS patterns show a major reduction of the intensity of the meridional scattering compared to the melt-spun fibers and very intense diffuse equatorial scattering. The WAXS patterns show a high level of c-axis orientation parallel to the fiber axis with both the a- and b-axes perpendicular to the fiber axis.

To further investigate the internal structure of the PE01, PE03, and PE07 fibers, we have peeled the fibers and taken SEM photomicrographs of their internal texture. Some of these are shown in Figure 7. It can be seen that the PE01 and PE03 fibers are highly fibrillated, particularly at draw ratios significantly greater than the NDR. PE07 seems to be less fibrillated than

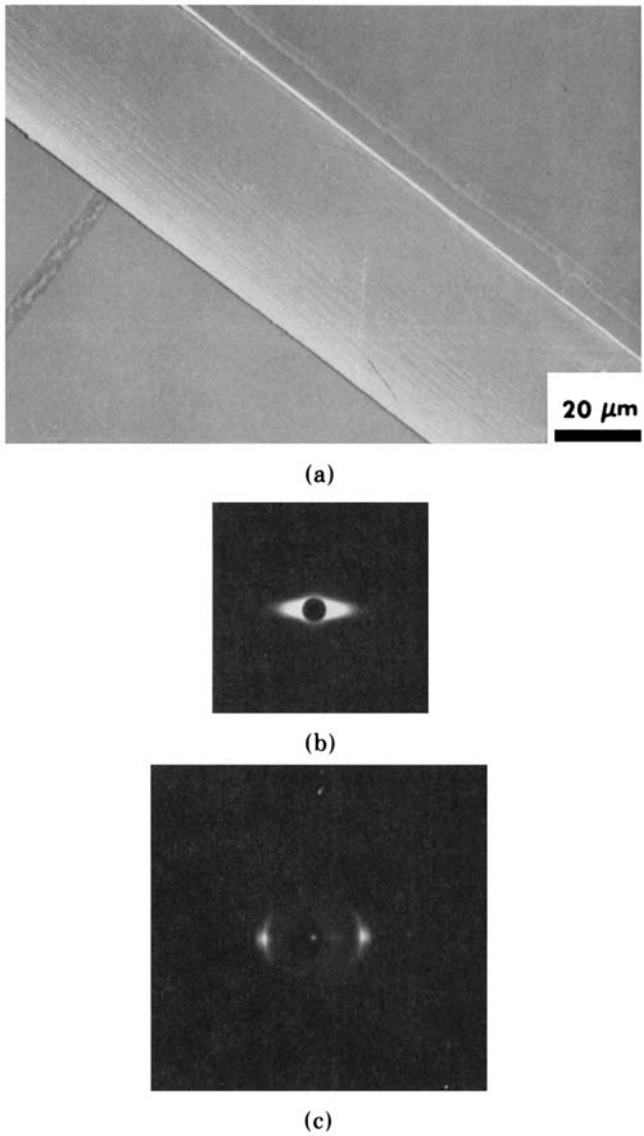

Fig. 6. Characterization of drawn (4×) PE07 fibers: (a) SEM photomicrograph; (b) SAXS pattern; (c) WAXS pattern.

the other two fibers. The degree of fibrillation clearly increases with increase in the draw ratios beyond the NDR.

As expected, drawing increased the Young's tangent modulus and the tensile strength of the fibers while decreasing the elongation to break. Typical values for the PE01 fiber with draw ratio 10 are a modulus of 22.2×10^9 dynes/cm^2, tensile strength of 48.1×10^8 dynes/cm^2, and an elongation to break of 75%. For the PE07 fiber with draw ratio 4, these values are 25.4×10^9 dynes/cm^2, 34.5×10^8 dynes/cm^2, and 122%, respectively. These may be compared to the values for melt-spun fiber shown in Table II. These results are similar to those reported earlier by White, Dharod, and Clark.[27]

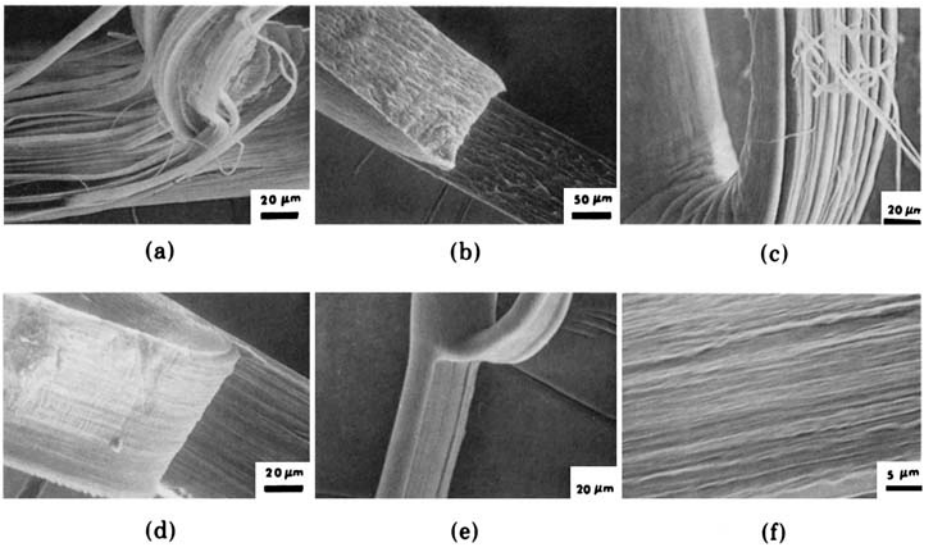

Fig. 7. SEM photomicrographs of peeled fibers: (a) PE03 drawn 10×; (b) PE03 drawn 5.2 × to NDR; (c) PE01 drawn 10×; (d) PE01 drawn 3 × to NDR; (e), (f) PE07 drawn 4×.

The SEM results and WAXS patterns suggest that the drawn fibers are highly crystalline, oriented, fibrillated structures in which the majority of polymer chains within the crystals and fibrils are parallel to the fiber axis. The crystalline orientation factors for the drawn fibers are of order

$$f_c \sim 0.95 \text{ and } f_a \sim f_b \sim -0.47. \tag{2}$$

In considering the changes in the SAXS patterns, we must bear in mind that x-ray scattering at small angles can be of two types,[31] discrete diffraction and diffuse scattering. Discrete diffraction at small angles is due to some periodicity in the electron density in the fiber which has a large spacing. Diffuse scattering has a maximum intensity at an angle of 0° and decreases in intensity out to 1–2°. It is caused by inhomogeneities of electron density. Unfortunately, the reciprocity principle[31,42] allows no way of distinguishing between the scattering from dense particles in a less dense medium and scattering from less dense particles in a denser medium. The scattering from these extreme systems will be equivalent if the density differences are the same. Thus, the equatorial diffuse scattering from our drawn fibers may be due to a distribution of elongated voids with major axes parallel to the fiber axis or to small microfibrils within the fibrils. The former view, for example, has been espoused by Statton.[43] Now studies by various researchers, e.g., White, Dharod, and Clark,[27] have found that the densities of drawn fibers measured in gradient density columns are substantially lower than those of the spun fibers despite minor increases in crystallinity as measured by calorimetry. This strongly suggests that the diffuse low-angle scattering is due to elongated microvoids.

The meridional scattering probably results from the superposition of some diffuse scattering from the voids and scattering from the remnants of the structure which gave intense meridional diffraction in the melt-spun fibers; i.e., the folded-chain lamellae. The decreased intensity of this contribution

must represent a severe (but incomplete) disruption of this morphology during the formation of the fibrils.

Peterlin[7,8] has proposed detailed mechanisms of the development of morphology in the drawn fibers including formation of microvoids and disruption of the lamellae. While these appear quite consistent with available experimental data, including the present results, they must still be considered in part speculative. It would seem to us, however, that the source of drawn fiber characteristics probably can be understood from purely phenomenological interpretation. Clearly, the character of the neck development process implies almost a discontinuous change in morphology which is also suggested by changes in orientation seen in WAXS patterns and the change not only in repeat distance but in intensity in SAXS patterns. The polymer in the neck is a very different material with considerably higher modulus than in the unnecked regions which gradually disappear as the filament is extended. One may indeed use the simple model of Orowan[44] and Chang and Lodge[45] to show this. Microdefects are always present, and when a quasi-transformation from a low modulus to a high modulus phase occurs, the complex stress field around such a defect near a phase boundary will result in its changing character to become a void elongated in the direction of stretch. The final result of this process is fibrillation whose extent increases with draw ratio. It is also to be remembered that small defects develop into microvoids in the uniaxial extension of polymeric glasses and metals and that neck development is also observed in these systems.

Twisted Spun Fibers

Twisting was carried out on both as-spun and on spun and drawn fibers. Although some previous work[18–20] has been reported dealing with the effect of twisting drawn fibers, no previous descriptions of the effects of twisting as-melt-spun fiber could be found. We shall consider these two cases consecutively, first presenting our results for as-spun fibers.

The melt-spun filaments were twisted various amounts up to 200 turns per inch (tpi) in the twist tester. WAXS and SAXS patterns were obtained and are shown in Figure 8 for the PE01 and PE07 filaments twisted 200 tpi. These patterns should be compared to those for the as-spun filaments, Figure 2. In the WAXS patterns, the diffracted intensity spreads more uniformly about the Debye rings for the twisted filaments; this is particularly noticeable for the 110 and 200 reflections. Also, a weak extra ring appears just inside the 110 reflection and corresponds to an interplanar spacing of 4.55 Å.

The extra ring is broad and weak in the present case, and for this reason its cause is somewhat uncertain. We believe that it is caused by the formation of a small amount of monoclinic form of polyethylene which has been reported by other investigators.[16,17,48] The interplanar spacing corresponds to the 001 reflection from the monoclinic form.* Furthermore, results to be

* The position of this reflection also happens to occur at the position where CuK_β radiation would be diffracted by orthorhombic (110) planes. However, exposures made on untwisted fiber for which the 110 orthorhombic CuK_β reflection was as strong or stronger than for the above twisted fiber exposures showed no extra reflection just inside the 110 reflection. Since these exposures were all made using the same geometry and filter, the observed extra reflection cannot be due to leakage of the CuK_β wavelength through the nickel filter.

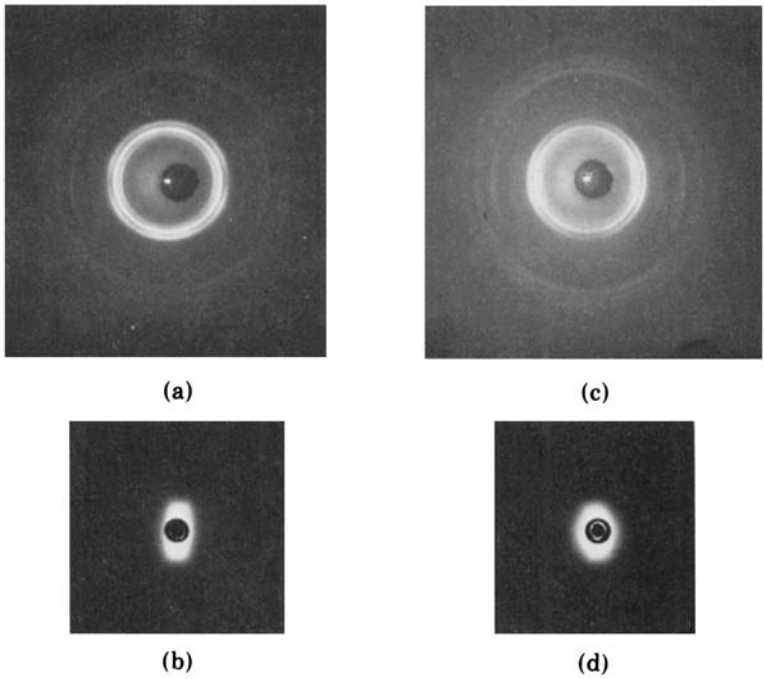

Fig. 8. X-ray diffraction patterns of spun and twisted filaments: (a) WAXS pattern of PE01 twisted 200 tpi; (b) SAXS pattern of PE01 twisted 200 tpi; (c) WAXS pattern of PE07 twisted 200 tpi; (d) SAXS pattern of PE07 twisted 200 tpi.

presented in the next section show a more distinctive crystalline reflection at this same position for twisted drawn fibers.

The SAXS patterns for the twisted filaments also differ from those of the initial melt-spun filaments. In particular, the meridional intensity decreases and a diffuse scattering component develops over it. For all practical purposes, the two-point diagram has disappeared. It must be presumed that the lamellar crystals and the amorphous regions are distorted and disoriented. The diffuse scattering again probably results from voids opened by the twisting.

The appearance of the filaments, as shown by SEM photomicrographs, are not appreciably changed from the as-spun case by twisting, and they thus are not given here.

The effect of twisting on the stress–strain curves is shown in Figure 9. Notice that the yield point which occurs in as-spun fiber is gradually removed by twisting. Associated with this is the disappearance of necking during elongation. The tensile strength and elongation to break both decrease as the twist level increases.

The above results may be interpreted in terms of the theory of plasticity.[47,48] The disappearance of the yield point results from the fact that plastic deformation of the fiber occurs during twisting. According to the simple theory of torsion,[49] a filament is uniformly twisted by an angle θ independent of radius resulting in a strain $r\theta$ and a shear stress $Gr\theta$, where G is the shear modulus. The stresses increase linearly then with radius. If we presume that plastic yielding is associated with a von Mises-type criterion,[47,48] then

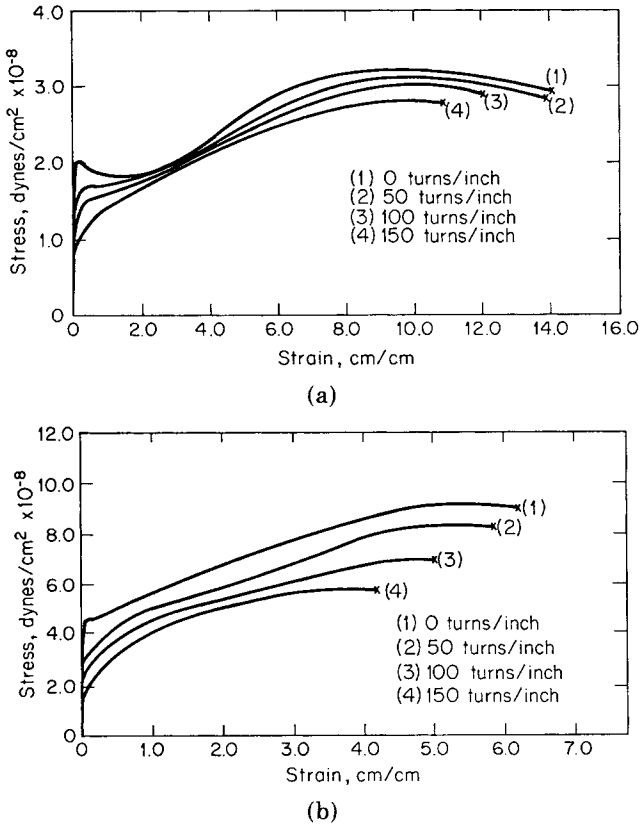

Fig. 9. Typical stress–strain curves for spun and twisted filaments: (a) PE01; (b) PE07.

twisting a filament can result in plastic yielding as well as tension. Furthermore, plastic yielding occurs in the twisted cylinder at a small twist angle in the outer radii of the cylinder. With additional twisting, the plastic yield point moves radially inward. Accordingly, if one tests the twisted fibers in tension, it would be expected that there would be a gradual removal of the yield point as measured on the whole filament. This is indeed the behavior observed.

Twisted Drawn Fibers

The *drawn fibers* also exhibit striking changes in their structure when twisted, as evidenced by their WAXS and SAXS patterns, Figure 10, and by SEM photomicrographs, Figure 11. From the photomicrograph Figure 11, it is clear that the fibrils created by drawing are twisted into a helical shape. Fibril twist angles (maximum) obtained from the SEM results are presented in Table III.

The SAXS patterns show intense equatorial diffuse scattering but its distribution changes as twist level increases. The breadth or lateral extent of the scattering normal to the fiber axis (along the equator) decreases, but it fans out parallel to the fiber axis.

The WAXS patterns are quite striking. The high level of axial orientation

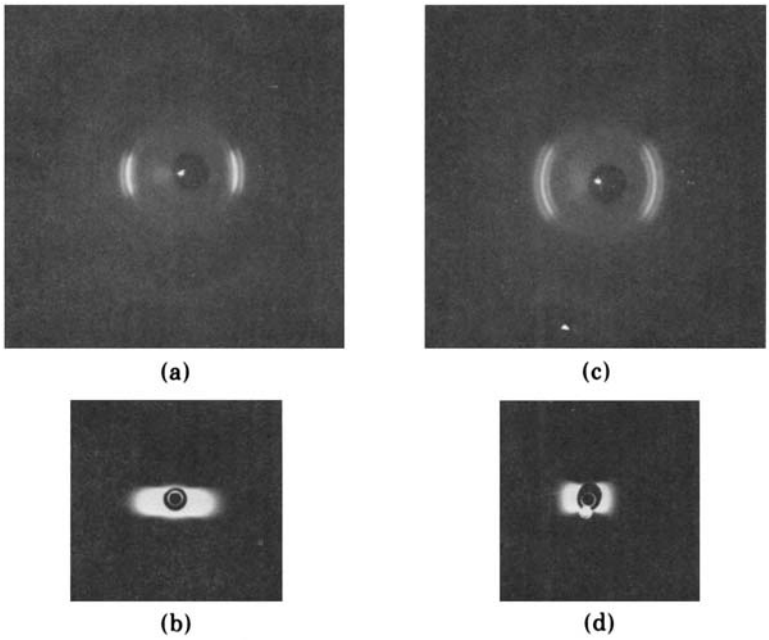

Fig. 10. X-ray diffraction patterns of drawn and twisted PE01 fibers: (a) WAXS, 50 tpi; (b) SAXS, 50 tpi; (c) WAXS, 100 tpi; (d) SAXS, 100 tpi.

seen in the drawn fibers is lost and the 110 reflection changes from an equatorial spot to a wide arc. At high twist levels, the extra reflection not expected on the basis of an orthorhombic unit cell occurs. In Figure 10c, in particular, it is clear that this is a sharp reflection from a second crystalline phase, presumably the monoclinic form of polyethylene.

The stress–strain curves of drawn and twisted PE01 fibers are shown in Figure 12 for various twist angles. For the PE01 fibers, there is a continuing decrease in Young's tangent modulus and tensile strength with extent of twist. The trend is similar in the PE07, except at the lowest twist angles where the modulus increases.

It would seem that there are two main effects of the twisting. First, it induces through slip or shear mechanisms a polymorphic transformation to yield a small amount of new crystalline phase, presumably the monoclinic polyethylene found by Kiho, Peterlin, and Geil[46] in single crystals and by Seto, Hara, and Tanaka[17] in transverse compression of oriented polymer and by Hein, Cooper, and Koutsky[18] on twisted drawn polyethylene fibers as in our experiments. Our 4.55 Å spacing plane corresponds to the observations of Seto et al. for the monoclinic (001) reflection. In this monoclinic cell, the polymer chain axis coincides with the b-axis. The unit cell parameters are a = 8.09 Å, b = 2.53 Å, c = 4.79 Å, and β = 107.9°. In the orthorhombic cell a = 7.40 Å, b = 4.94 Å, and c = 2.54 Å (chain axis direction).[21] This polymorphic transformation occurs to a limited degree in both as-spun and spun and drawn fibers when twisted.

The second feature is the disorientation which results from twisting. For the drawn fibers this is accompanied by a helical twisting of the fibrillar superstructure as revealed by SEM. The decreased orientation shown by the WAXS patterns may be explained by considering the polyethylene chains to

Fig. 11. SEM photomicrograph of the surface of PE01 fiber, drawn 10× and twisted 100 tpi.

lie along the fibrillar axes. The change in the distribution of diffuse scattering in the SAXS patterns probably corresponds to tilting and perhaps distortion and lateral compression of microvoids during twisting.

A quantitative model of the twisted drawn fibers may be obtained by noting the similarity of this twisted fibrillar structure to a continuous filament textile yarn (see Fig. 13). Gegauff,[50] Platt,[51] Hearle,[2,52] and others[2,53] have developed a mathematical model for continuous filament yarns to predict their deformation behavior and stress–strain curves. This model may readily be adapted to a fiber consisting of continuous twisted fibrils and used to predict both the character of the WAXS diagrams and stress–strain curves. This CTFY theory (continuous twisted fibril yarn) presumes the fibrils have the same crystalline character and mechanical properties as the drawn yarn and the variations in WAXS patterns and mechanical properties of the twisted fiber are purely geometric in nature. The CTFY model assumes that the fibrils are distributed across the yarn with the same twist factor T (turns per unit length). Thus, the twist angle ϕ (see Fig. 13) varies with radius according to

$$\tan \phi = \frac{2\pi r}{h} = 2\pi r T \tag{3}$$

and decreases from a maximum of $\tan^{-1} 2\pi RT$ at the outer radius of the fiber

TABLE III
Comparison of Maximum Twist Angle Measured by SEM with Computed Values and Results from X-Ray Diffraction

Fiber	Twist, tpi	ϕ_{max} SEM	ϕ_{max} WAXS	ϕ_{max} Calculation[a]
PE01	50	22°	20°	22.6
	75	31°	30°	32.0
	100	42°	35°	39.8
PE07	25	7°	6°	7.9
	50	15°	12°	15.6
	150	38°	30°	40.0

[a] From eq. (3).

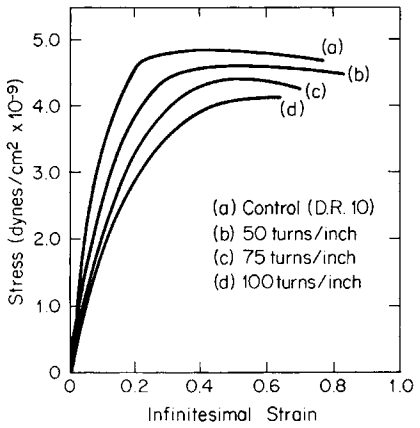

Fig. 12. Typical stress–strain curves for drawn and twisted PE01 fibers.

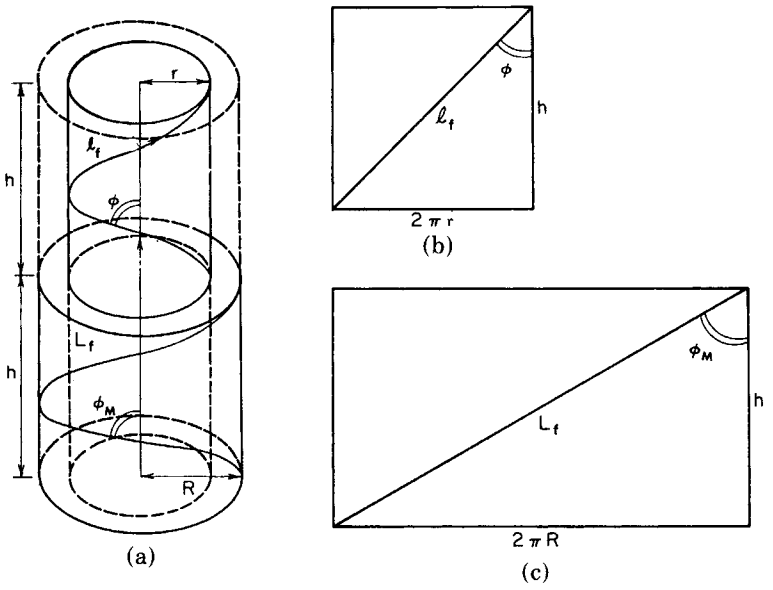

Fig. 13. Continuous-filament yarn model of a twisted fiber, with fibrils assumed to lie in a helical configuration.

to zero at the fiber axis. In predicting mechanical properties, the CTFY model requires the fibrils to deform independently of each other.

The azimuthal variation, angle ψ, of intensity around the Debye rings in the WAXS patterns follows directly from the geometry and turns out to be equivalent to the model used by Cooper, McKinnon, and Prevorsek.[19,20] We wish to obtain ψ as a function of ϕ. When ϕ is zero, ψ will be zero. The relationship between ψ, the Bragg angle θ and the angle ϕ is approximately

$$\sin \psi = \frac{1}{\cos \theta} \sin \phi. \tag{4}$$

One may also compute the azimuthal intensity distribution around the Debye

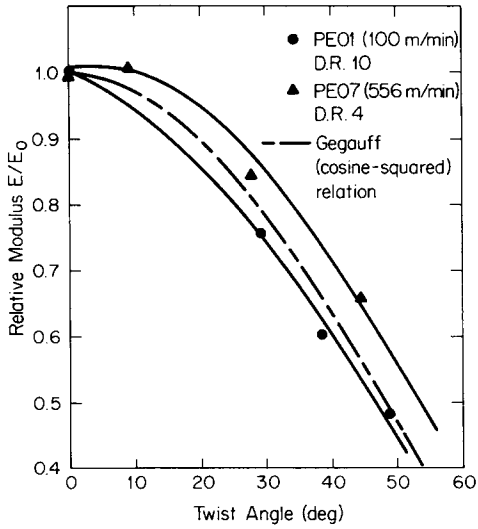

Fig. 14. Reduced tangent modulus E (twisted)/E (drawn) as a function of SEM twist angle.

arcs.[19,20] We will concern ourselves here with computation of ϕ_{max} from ψ_{max} and comparison with results measured in SEM photomicrographs and as computed from eq. (3). These calculations are summarized in Table III. The agreement is good at the lower twist angles, but the WAXS measurements tend to be too low at the higher twist angles.

The CTFY model can also be applied to the tangent modulus E of the twisted fibers. Various theories of the modulus of continuous-filament textile yarns have been developed through the years,[2,50–53] and considerable data have been obtained.[2] The experimental data and the more sophisticated theories turn out to be well represented by the simplest and earliest of theories, that of Gegauff,[50] which presumes that the individual filaments obey Hooke's law in tension and neglects lateral pressure effects (which influence filament tension). Using the Gegauff approximation in the CTFY model, we obtain

$$\frac{E \text{ (twisted fiber)}}{E \text{ (drawn fiber)}} = \cos^2 \phi_{max}. \tag{5}$$

In Figure 14, we plot the modulus ratio of eq. (5) versus SEM ϕ_{max} and include Gegauff's cosine-squared law. The agreement is reasonable.

Heat-Set Fibers

"As drawn" and "drawn and twisted" PE01 and PE07 fibers were heat set at 120°C for 30 min. Representative WAXS and SAXS patterns are presented in Figures 15 and 16. In Figure 17, we see that the most obvious effect of heat setting the twisted fibers is to remove the extra reflection (d = 4.55 Å) within the 110 reflection. The SAXS patterns exhibit both meridional and equatorial scattering. Compared to the as-drawn or as-twisted fibers, the intensity of the diffuse equatorial scattering is reduced while the meridional scattering is increased. The decrease in equatorial scattering must be due to

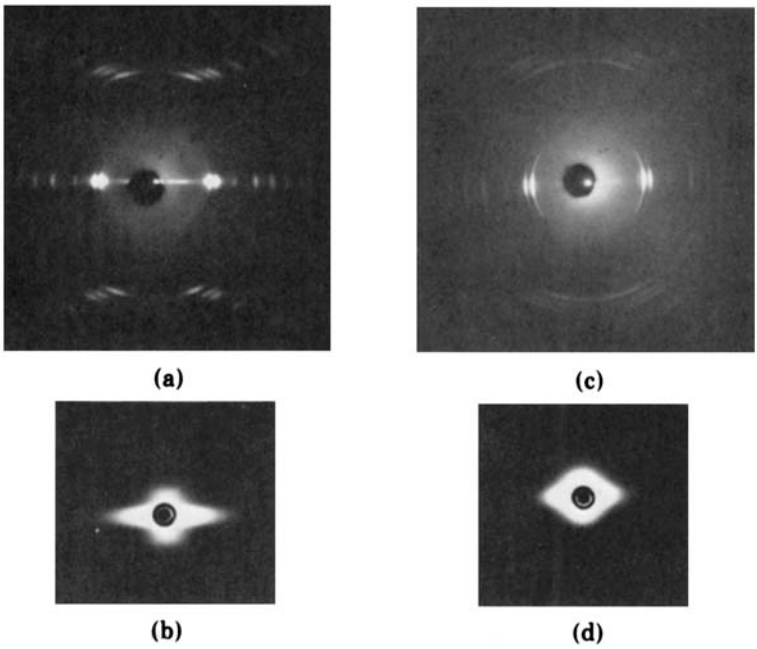

Fig. 15. X-ray diffraction patterns of drawn and heat-set (30 min at 120°C) fibers: (a) WAXS, PE01, drawn 10×; (b) SAXS, PE01, drawn 10×; (c) WAXS, PE07, drawn 4×; (d) SAXS, PE07, drawn 4×.

the healing of microvoids. There was no noticeable change in the SEM photomicrographs of the fiber surfaces. Observation of peeled, drawn, and heat-set fibers showed that the structure was still highly fibrillated. The degree of fibrillation did not appear to have decreased due to the annealing treatment, as shown in Figure 17. The mechanical properties of the heat-set fibers showed trends similar to those presented in Figure 12, although there were small improvements in the tensile strength and modulus together with a decrease in the elongation to break. The changes in these quantities are summarized in Table IV for the PE01 fiber.

The observed changes in WAXS, SAXS, and mechanical properties indicate that the primary effects of heat setting are to heal small defects in the fiber structure and to transform the monoclinic phase back to the orthorhombic form. Geil[54] observed a similar disappearance of the monoclinic phase in single crystals after annealing at 120°C.

Untwisted Fibers

Figure 18 shows WAXS and SAXS patterns of PE01 fibers which were forcibly untwisted after the heat-setting operation described in the previous section. It is observed that the equatorial areas on the WAXS patterns return back to spots similar to the original equatorial spots as if no twist had ever been imparted to the fibers. Note, however, that the diffraction patterns of Figure 18 do not compare as well with Figure 5, the patterns for the as-drawn samples, as they do with Figure 15, the patterns for drawn and heat-set samples. Thus, the effects of heat setting on the WAXS and SAXS patterns are

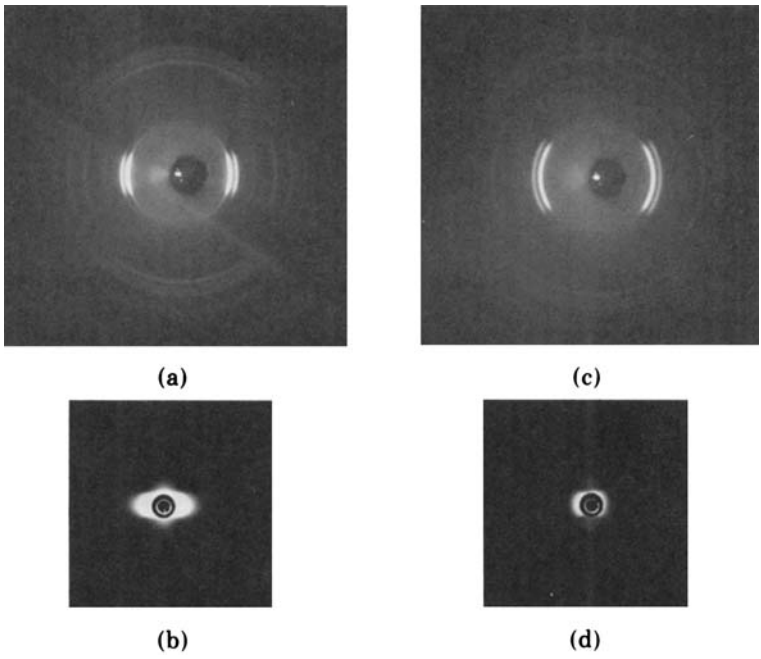

Fig. 16. X-ray diffraction patterns of drawn, twisted, and heat-set (20 min at 120°C) PE01 fibers: (a) WAXS, 50 tpi; (b) SAXS, 50 tpi; (c) WAXS, 100 tpi; (d) SAXS, 100 tpi.

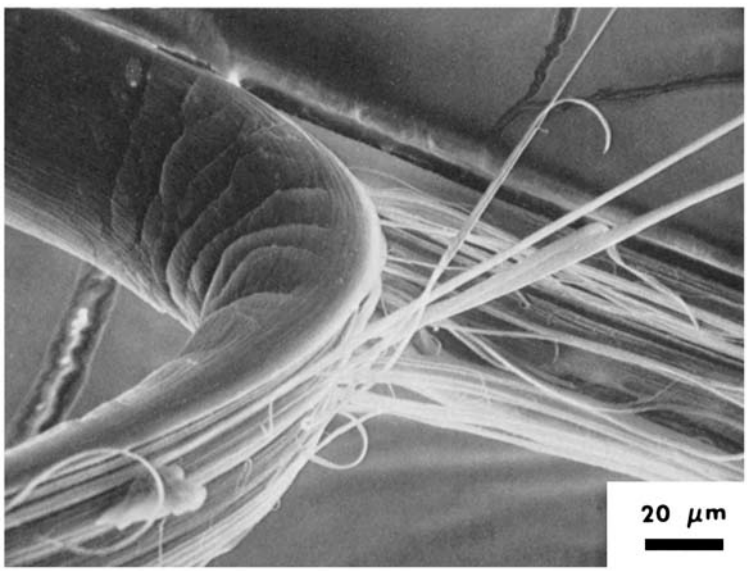

Fig. 17. PE01 fiber drawn 10× and heat set for 30 min at 120°C.

largely retained after untwisting. It is interesting that untwisting of the heat-set fiber causes an increase in both the meridional and the equatorial scattering as compared to the twisted, heat-set fiber (compare Figs. 18b and 18d with Figs. 16b and 16d).

In spite of the similarities between the x-ray patterns of untwisted fibers to

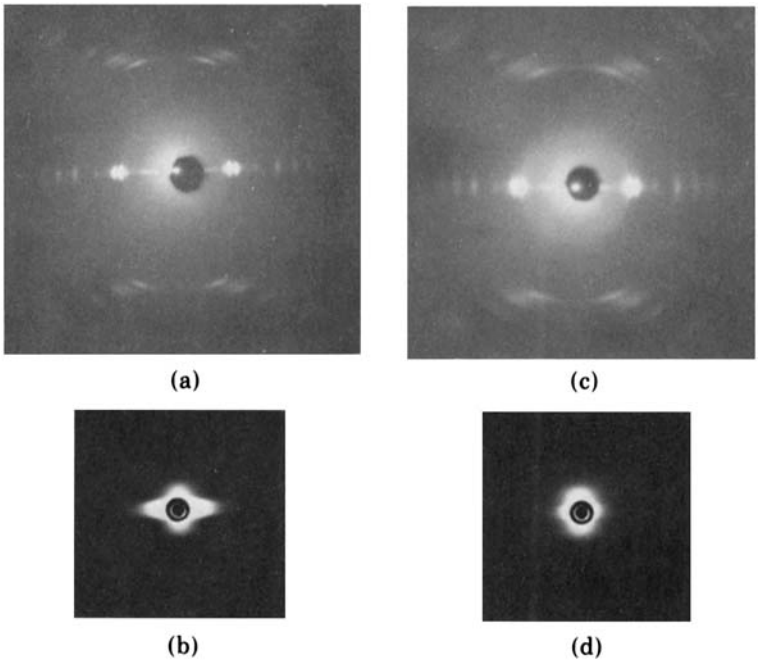

Fig. 18. X-ray diffraction patterns of forcibly untwisted PE01 fibers which were initially drawn 10×, twisted, and heat set 30 min at 120°C: (a) WAXS, 50 tpi; (b) SAXS, 50 tpi; (c) WAXS, 100 tpi; (d) SAXS, 100 tpi.

those of samples which were never twisted, the effects of twisting are not reversible. The best evidence for this is shown in Figure 19, which shows SEM photomicrographs of the PE01 and PE03 fibers. Here, it is observed that the fibrils contain endless stacks of kink bands (note zigzag nature of fibrils). These kink bands can be observed somewhat better after etching the sample in fuming nitric acid at 80°C for 1 hr as in Figure 19b. They can also be observed on the internal fibrils upon peeling, Figure 19c.

Kink band formation in complex deformations of oriented polyethylene has been observed by several researchers.[12–15] Compression of oriented samples is one established method of creating kink bands. Untwisting of the twisted fibrillar structure may place the outer layers of fibrils in compression. Other modes of deformation may also cause kink band formation. Kink band formation in untwisted fibers has been reported by Hien, Cooper, and Koutsky[18] and Dr. Y. Tajima informs us of work of Professor M. Kurokawa of the Kyoto University of Industrial Arts and Textiles.*

The stress–strain curves for the untwisted PE01 fibers have a very similar appearance to those of the twisted (Fig. 12) or twisted and heat-set fibers. The tensile strength, modulus, and elongation to break of the untwisted fiber again decreases with the amount of original twist as compared to the control. The control is a drawn fiber which was heat set at constant length but never twisted. In general, the untwisted fibers also exhibit lower tensile strength,

* Prof. Kurokawa has recently supplied us with a copy of the paper containing this work. M. Kurokawa, T. Konishi, F. Taki, and S. Fujii, *Kobunshi Ronbunshu,* (in Japanese) **31** (1), 74–78 (1974).

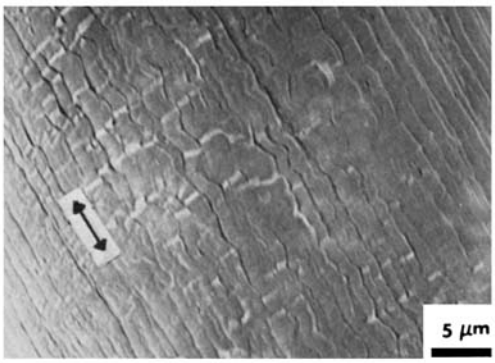

(a)

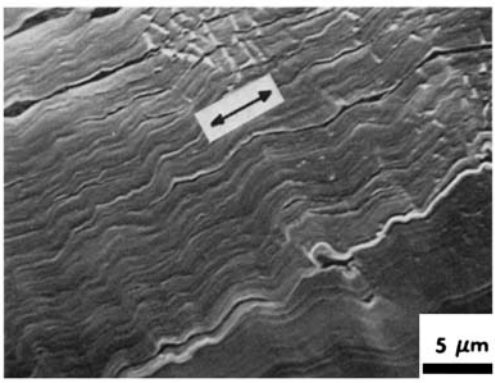

(b)

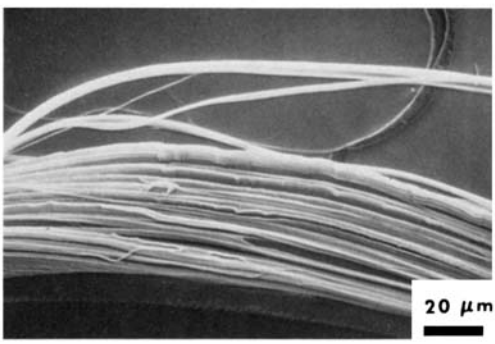

(c)

Fig. 19. Kink bands in untwisted fibers: (a) surface of PE01 fiber, drawn 10×, twisted 100 tpi, heat set, and untwisted; (b) surface of PE03 fiber after etching for 1 hr in nitric acid at 80°C; Sample was drawn 10×, twisted 125 tpi; (c) appearance of peeled area of fiber shown in (a).

modulus, and elongation to break than their twisted and heat-set counterparts. Table IV presents a comparison of these values.

These results show that defects created by twisting and untwisting result in premature fracture. The fact that untwisted fibers do not regain their original pretwisted properties, but actually have lower properties than their twisted and heat-set counterparts, indicates that the defects cannot be removed but are further enhanced by untwisting. The fact that the CTFY model

TABLE IV
Comparison of Modulus, Elongation to Break, and Tensile Strength of PE01 Fibers

Condition	As-drawn and twisted			Heat set 30 min @ 120°C after twisting			Untwisted after heat setting		
Amount of twist, tpi	Modulus, (dynes/cm^2) $\times 10^{-9}$	Elongation to break, %	Tensile strength, (dynes/cm^2) $\times 10^{-9}$	Modulus, (dynes/cm^2) $\times 10^{-9}$	Elongation to break, %	Tensile strength, (dynes/cm^2) $\times 10^{-9}$	Modulus, (dynes/cm^2) $\times 10^{-9}$	Elongation to break, %	Tensile strength, (dynes/cm^2) $\times 10^{-9}$
0	22.2	75	4.8	25.0	59	5.8	25.0	59	5.8
50	20.4	84	4.6	23.5	61	5.7	21.0	53	5.2
75	14.3	71	4.4	20.5	40	5.5	17.4	47	4.6
100	11.1	65	4.1	17.7	44	4.8	13.3	40	3.9

gives reasonable predictions for the twisted fibers suggests that most of the defects are of a type which tends to separate the fiber into its individual fibrils. The modulus of the untwisted fiber is, according to this model, essentially the same as the modulus of the individual fibrils. The lack of recovery of the modulus and the further deterioration of properties by untwisting is not accounted for on the basis of the CTFY model.

SUMMARY AND CONCLUSIONS

The major results and the conclusions drawn from this study are briefly summarized below.

1. The behavior and response of melt-spun polyethylene filaments during further processing operations such as drawing, twisting, heat setting, and untwisting depends on the spinning conditions used in the production of the filaments. This was attributed to the difference in morphology developed by different spinning conditions.

2. Drawing at room temperature proceeds by necking. The tensile curve exhibits a yield point and extension to the "natural draw ratio" at nearly constant load. Both the natural draw ratio and the total elongation to break are greater for fibers spun at low stress, i.e., low take-up velocity, than at high stress.

3. Drawing results in a very high crystalline orientation in which the c-axes of the polyethylene crystals are essentially parallel to the fiber axis. Drawing also results in fibrillation and increases in modulus and tensile strength. The amount of fibrillation as observed in SEM photomicrographs increases with total draw ratio. At a draw ratio slightly greater than the natural draw ratio, the amount of fibrillation decreases with increasing take-up velocity during spinning.

4. Twisting of either as-spun or drawn fibers decreased the axial orientation, modulus, tensile strength, and usually also the elongation to break. The change in these properties increased with increasing twist angle. Twisting also caused a transformation of a small fraction of the sample to the monoclinic crystal structure.

5. For as-spun filaments, twisting tended to remove the yield point and produce a more uniform elongation when the twisted fiber was loaded in tension.

6. A model suggested by the geometry of continuous filament yarns gave a reasonable prediction of the decrease in relative modulus and axial orientation due to twisting of drawn fibers.

7. Heat setting caused partial healing of elongated voids which were generated during drawing, increased the perfection and periodicity of the stacking of lamellar crystals, and caused the monoclinic polyethylene formed during twisting to transform back to the orthorhombic crystal modification. Heat setting also increased the modulus and tensile strength of the fibers but decreased the elongation to break.

8. Untwisting returned the crystalline orientation in the fiber to essentially that which it would have if it had not been twisted. However, scanning electron microscopy examination showed that the fibrils were not simply returned to their untwisted form, but that they contained numerous kink

bands. Untwisting also resulted in further deterioration of the mechanical properties.

This research was supported in part by the National Science Foundation under NSF Grant GK-18897. The help of Professor Charles Noel, Department of Textiles and Clothing, is acknowledged. Professor Noel also made the twist tester available.

References

1. R. W. Dent and J. W. S. Hearle, *Text. Res. J.*, **30,** 805 (1960).
2. J. W. S. Hearle, P. Grosberg, and S. Backer, *The Structural Mechanics of Fibers, Yarns and Fabrics,* Vol. 1, Wiley-Interscience, New York, 1967.
3. G. D. Wilkinson, Ed., *Textured Yarn Technology,* Monsanto, Decatur, 1967.
4. G. D. Wilkinson, Ed., *Draw Textured Yarn Technology,* Monsanto, Decatur, 1974.
5. R. L. Smith, R. Pieters, and M. E. Morrison, *Trans. Soc. Rheol.*, **10,** 556 (1972).
6. W. H. Carothers, and J. W. Hill, *J. Amer. Chem. Soc.*, **54,** 1579 (1932).
7. A. Peterlin, in *Man-Made Fibers,* Vol. 1, H. Mark, S. Atlas, and E. Cernia, Eds., Wiley, New York, 1967.
8. A. Peterlin, in *Advances in Polymer Science and Engineering,* K. D. Pae, D. R. Morrow, and Y. Chen, Eds., Plenum, New York, 1973.
9. J. D. Muzzy and D. Hansen, *Text. Res. J.*, **41,** 436 (1971).
10. R. D. Van Veld, G. Morris, and H. R. Billica, *J. Appl. Polym. Sci.*, **12,** 2709 (1968).
11. D. A. Zaukelies, *J. Appl. Phys.*, **33,** 2797 (1962).
12. M. Kurokawa and T. Ban, *J. Appl. Polym. Sci.*, **8,** 971 (1964).
13. T. Seto and Y. Tajima, *Jap. J. Appl. Phys.*, **5,** 534 (1966).
14. R. E. Robertson, *J. Polym. Sci.*, **7,** 1315 (1969).
15. Y. Tajima, *Jap. J. Appl. Phys.*, **12,** 40 (1973).
16. F. C. Frank, A. Keller, and A. O'Conner, *Phil. Mag.*, **3,** 64 (1958).
17. T. Seto, T. Hara, and K. Tanaka, *Jap. J. Appl. Phys.*, **7,** 31 (1968).
18. N. V. Hien, S. L. Cooper, and J. A. Koutsky, *J. Macromol. Sci.-Phys.*, **B6,** 343 (1972).
19. S. L. Cooper, A. J. McKinnon, and D. C. Prevorsek, *J. Polym. Sci. A-1,* **6,** 353 (1968).
20. S. L. Cooper, A. J. McKinnon, and D. C. Prevorsek, *Text. Res. J.*, **38,** 803 (1968).
21. C. W. Bunn, *Trans. Faraday Soc.*, **35,** 482 (1939).
22. D. Acierno, J. N. Dalton, J. M. Rodriguez, and J. L. White, *J. Appl. Polym. Sci.*, **15,** 2395 (1971).
23. I. J. Chen, G. E. Hagler, L. E. Abbott, D. C. Bogue, and J. L. White, *Trans. Soc. Rheol.*, **16,** 473 (1972).
24. J. E. Spruiell, D. E. McCord, and R. A. Beuerlein, *Trans. Soc. Rheol.*, **16,** 535 (1972).
25. L. E. Abbott and J. L. White, *Appl. Polym. Symp.*, **20,** 247 (1973).
26. J. R. Dees and J. E. Spruiell, *J. Appl. Polym. Sci.*, **18,** 1053 (1974).
27. J. L. White, K. C. Dharod, and E. S. Clark, *J. Appl. Polym. Sci.*, **18,** 2539 (1974).
28. J. E. Spruiell and J. L. White, *Polym. Eng. Sci.*, **15,** 660 (1975).
29. R. G. Scott, ASTM Special Technical Publication No. 257, 1959, p. 121.
30. J. T. Sparrow, in *The Use of the Scanning Electron Microscope,* J. W. S. Hearle, J. T. Sparrow, and P. M. Cross, Eds., Pergamon, Oxford, 1972, p. 151Gf.
31. L. E. Alexander, *X-Ray Diffraction Methods in Polymer Science,* Wiley, New York, 1969.
32. J. J. Hermans, P. H. Hermans, D. Vermeas, and A. Weidinger, *Rec. Trav. Chim.*, **65,** 427 (1956).
33. R. S. Stein, *J. Polym. Sci.*, **31,** 327 (1958).
34. R. S. Stein, *J. Polym. Sci.*, **31,** 335 (1958).
35. A. Keller, *Phil. Mag.*, **2** (8), 1171 (1957).
36. P. H. Till, *J. Polym. Sci.*, **24,** 361 (1957).
37. C. W. Bunn and T. C. Alcock, *Trans. Faraday Soc.*, **41,** 317 (1945).
38. W. M. D. Bryant, *J. Polym. Sci.*, **2,** 547 (1947).
39. A. Keller, *J. Polym. Sci.*, **17,** 351 (1955).
40. A. J. Pennings and A. M. Kiel, *Kolloid-Z.Z. Polym.*, **205,** 160 (1965).
41. A. Keller and M. Machin, *J. Macromol. Sci.-Phys.*, **1,** 41 (1967).
42. M. Born, and E. Wolf, *Principles of Optics,* 4th ed., Pergamon, Oxford, 1970.

43. W. O. Statton, *J. Polym. Sci.*, **41,** 143 (1959).
44. E. Orowan, *Rept. Progr. Phys.*, **12,** 185 (1949).
45. H. Chang, and A. S. Lodge, *Rheol. Acta*, **10,** 448 (1971).
46. H. Kiho, A. Peterlin, and P. H. Geil, *J. Appl. Phys.*, **35,** 1599 (1964).
47. A. Nadai, *Theory of Flow and Fracture of Solids*, McGraw-Hill, New York, 1950.
48. R. Hill, *The Mathematical Theory of Plasticity*, Clarendon Press, Oxford, 1950.
49. S. Timoshenko and J. N. Goodier, *Theory of Elasticity*, 2nd ed., McGraw-Hill, New York, 1951.
50. C. Gegauff, *Bull. Soc. Ind. Mulhouse*, 153 (April 1907).
51. M. M. Platt, *Text. Res. J.*, **20**, 1 (1950).
52. J. W. S. Hearle, *J. Text. Inst.*, **41,** T389 (1958).
53. C. C. Cheng, J. L. White, and K. E. Duckett, *Text. Res. J.*, **44,** 483 (1974).
54. P. H. Geil, *J. Polym. Sci.*, **A2,** 3835 (1964).

Received August 21, 1975